Flexible Shaft as Remote and Elastic Transmission for Robot Arms

Muhammad Usman*[,1,2], Thierry Hubert[1,3], Amin Khorasani[1,3], Raphaël Furnémont[1,3], Bram Vanderborght[1,2], Dirk Lefeber[1,3], Greet Van de Perre[1,2] and Tom Verstraten[1,3]

***Abstract*—Research on human-friendly robots focuses on safety through software and hardware. Hardware-based safety offers a significant advantage over software-based safety if an accurate hardware model is integrated into the solution. Design of elastic and off-joint actuation has established safety by hardware, where the inherent qualities of elastic and lightweight nature make the robot safe for interaction. Combining series elastic actuators with cable/belt pulley-based remote transmission offers inherently safe hardware design, albeit with increased design and modeling complexity. This paper introduces remote and elastic actuation as a single-element solution for robot arm design using a flexible shaft. The test-bench approach studies the remote and elastic effects of a flexible shaft-based transmission for a robot. A set of nine flexible shafts, differing in length and diameter, are used for benchmarking as 3-D surface empirical maps to facilitate their optimal selection for robot design. An example 3 Degree Of Freedom (DOF) robot arm using a flexible shaft as a remote and elastic actuator is designed and modeled. A low-level control based on a flexible shaft is proposed, backed by the experimental results.**

***Index Terms*—Compliant Joints and Mechanisms, Actuation and Joint Mechanisms.**

I. INTRODUCTION

ENGINEERS and researchers are diligently advancing robotics for safe human-robot interaction. Safety in robotics hinges on environment-aware design and compliant mechanics. Robot's torque control [1] [2] has been introduced to achieve high performance by accurate torque sensing. Such sensing allows the robot to overcome the non-linearities and friction due to the gearbox employed in the actuation system, resulting in virtually high back-drivability and compliance in robots. Based on the technology, a set of robotic manipulators developed with built-in compliance due to harmonic reducer, harnessed for torque sensing using strain gauges [3]. Although the torque control has successfully lowered the effective impedance of robots, the inherent characteristics of high impedance due to rigid mechanical design make it difficult for the technology to achieve safety without an active control layer.

To mitigate safety limitations in high impedance actuators, elasticity is introduced between the actuator output and the load, reducing impedance and improving safety and energy efficiency [4] [5]. Elastic actuation, with its advantages, possesses limitations in high-speed performance [6]. However, their safety features drive exploration into variable stiffness actuators [7] to reap the benefits of both low and high stiffnesses at the cost of mechanical complexity and low affordability. Another method for enhancing inherent safety is to decrease the overall moving mass of the robot through remote actuation, reducing effective inertia and energy consumption. Cable-driven manipulators [8] [9] offer good performance and safety but with increased mechanical complexity and maintenance due to strings' creep and slack.

Combining elastic and cable-driven actuation in manipulator design [10] achieves low effective mass for high-speed, safe operation, albeit with increased design, modeling, and control complexity. Zinn et al. [11] introduced a macro-mini approach, using small on-joint motors for high-frequency tasks and cable pulley with spring element for low-frequency tasks. Shin et al. [12] adopted a similar concept with pneumatic actuators to reduce mechanical complexity compared to cable-driven elastic actuation. While these combinations enhance robotic performance, they introduce mechanical complexity and control challenges.

Cianca et al. [13] presented a Remote and Torsionally Compliant Actuator (RTCA) for wearable robots, showcasing the unified use of remote and elastic actuation with flexible shafts. Flexible shafts, valued for compactness and simplicity, have found applications in surgical robotics, including tools for colonoscopes [14] [15]. Liu et al. [16] developed a soft gripper with flexible shafts, offering bending compliance and torsional stiffness for grasping and in-hand cap manipulation. As a unified solution of remote and series elasticity, flexible shafts hold the potential for various robotics applications. Research work in [13], [16] focuses on the design-specific empirical study only to facilitate design and control in their robots. Hence, there is a lack of benchmarking of the torsional and bending characteristics of flexible shafts in relation to their physical dimensions. Such benchmarking of flexible shafts based on the design parameters of diameter and length can facilitate the design of an optimal actuator for the target application. Furthermore, there is no study on the series and parallel

Manuscript received: November, 29, 2023; Revised January, 29, 2024; Accepted March, 29, 2024.

This paper was recommended for publication by Editor J.P. Desai upon evaluation of the Associate Editor and Reviewers' comments. This work was supported by Research Foundation Flanders (FWO) SBO project ELYSA Project (grant number S001821N).

[1,2]Muhammad Usman, Bram Vanderborght and Greet Van de Perre are with Brubotics, Vrije Universiteit Brussel and imec, Belgium. {muhammad.usman, bram.vanderborght, greet.van.de.perre}@vub.be

[1,3]Thierry Hubert, Amin Khorasani, Raphaël Furnémont, Dirk Lefeber and Tom Verstraten are with Brubotics, Vrije Universiteit Brussel and Flandersmake, Belgium. {thierry.hubert,amin.khorasani,raphael.furnemont, dirk.lefeber,tom.verstraten}@vub.be

Digital Object Identifier (DOI): see top of this page.

compliance of flexible shaft in the robots studied before, which is an important characteristics to study separately and in detail.

Hence, this paper studies the transmission of torque to a distal joint across a robot joint using a flexible shaft, employing the bending and torsional compliance for series and parallel elastic effects (discussed in Section II-C) to the distal and preceding joint, respectively. The study thoroughly investigates the compliance effects of the flexible shaft on a test bench using nine flexible shafts varying in length and diameter with the common material (carbon steel) and same construction. Subsequently, a 3-degree-of-freedom robot in anthropomorphic configuration is developed using a flexible shaft as a transmission and elastic element for the third distal joint. A selection procedure of flexible shafts is provided for desired elasticity.

The paper is organized as follows: In Section II, the paper discusses the characteristics of a flexible shaft with its effects on a robot arm. In Section III, the experimental investigation of flexible shaft-based transmission and elastic element for robot arm using a test bench are provided and discussed. Section IV discusses the 3-DOF robot developed using a flexible shaft in three subsections: design, modeling, and control. Section V discusses the research outcome and concludes the paper with future work propositions.

II. Flexible Shaft

A. Construction of Flexible Shaft

The flexible shaft is constructed by tightly winding multiple wire coils of variable radius of helices on top of each other around a core wire as shown in Figure 1(a) and (b). The winding direction of adjacent coils is kept opposite to give a bi-directional transmission potential as shown in Figure 1(a). With the increased radius of wires and the flexible shaft's global radius, $D/2$ as shown in Figure 1(a), the torque transmission capability is increased at the cost of less bending compliance. Like traditional springs, the increase in length, L and decrease in diameter, D results in decreased torsional and bending stiffness.

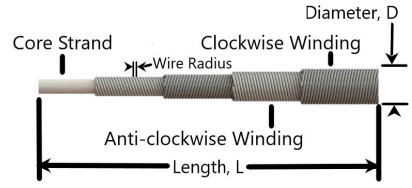

(a) Schematics

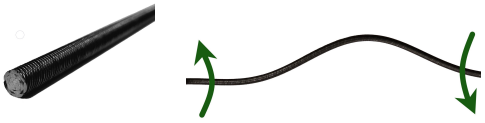

(b) Isometric View. (c) Helical Buckling.

Fig. 1. Flexible Shaft Construction and Characteristics

Due to its bending compliance, once a torque is transmitted, it undergoes a helical buckling, as shown in Figure 1(c), causing reaction pull forces on the motor and load attachments. To stabilize this behavior, a geometric constraint-based stiffness is introduced around the flexible shaft as a flexible conduit with bearings at the end for relative rotation, as shown in Figure 2. The conduit ends are designed to provide connection fixtures for the source and load ends. A conduit with a high torsional and low bending stiffness is an ideal selection for the flexible shaft. The conduit used is made of rubber sheath and flat strip metal coil, which restrains the helical buckling of flexible shaft to assist the transmission of torque.

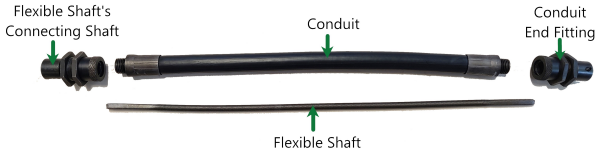

Fig. 2. Flexible Shaft with Conduit and End Fittings.

The coil layers of the flexible shaft being tightly wound undergo an elastic contact instead of rubbing against each other. Depending on the direction of applied torque and winding direction, the coils try to wind or unwind in the outermost layer. This kinetic direction-dependency nature makes flexible shafts possess an asymmetrical nature for the direction of torque transmission.

B. Robot Arm Topology

To fully leverage the transmission capabilities of a flexible shaft as a remote and series elastic transmission, the optimal arrangement involves transmitting torque over the robot joint to a distal joint, utilizing its bending compliance, illustrated in Figure 3. It is preferable to position the actuation unit at the base of the robot to achieve effective low inertia of the moving mass of the robot.

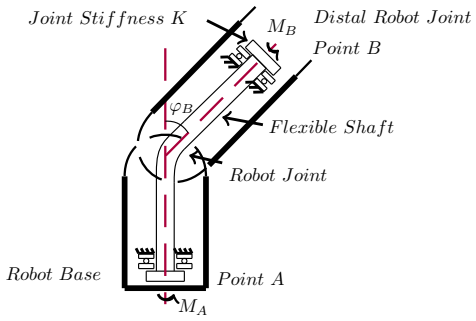

Fig. 3. Robot Topology Using Flexible Shaft.

Among the most commercially available robot arms, like the KUKA arms and Universal Robots UR series, the most adapted kinematic structure is an anthropomorphic robot arm with the body joint axis perpendicular to the fixed platform and shoulder-elbow joints parallel to it. As shoulder and elbow joints are significant contributors to the payload manipulation; thus, an elbow joint is considered to be vital for effective remote actuation with a flexible shaft passing over the shoulder joint. In this topology, the mass of the actuator unit is moved to link 1, which is effectively the robot's base, reducing the robot's effective mass.

C. Effects of Flexible Shaft on Robot

Due to its construction of tightly wounded coils, a flexible shaft offers torsional and bending elasticity if routed across a joint for power transmission. The sections below discuss the torsional and bending elasticity as series and parallel elastic effects on the robot joints.

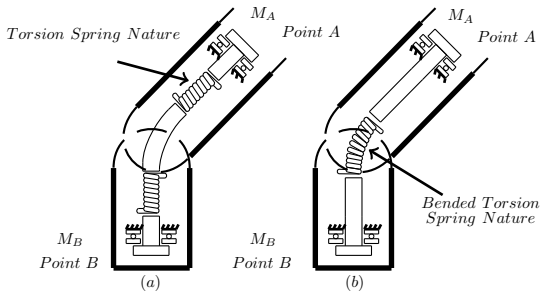

Fig. 4. a) Series Elasticity at Distal Joint. b) Parallel Elasticity at Preceding Joint.

1) Series Elastic Effect: The series elasticity exists due to the helical torsion spring-like nature of the tightly wounded coils on top of each other, as shown in Figure 4 a). This series elasticity is in series with the distal joint motor driving the flexible shaft. A set of two torsional mass-spring-damper models is considered to comprehend the asymmetrical behavior of flexible shafts due to the winding and unwinding of the outermost coil under torsion. The positive direction of the twist angle $\Delta\theta$ is defined in the direction of the outermost coil's winding of the flexible shaft. A separate set of stiffness and damping coefficients are considered for each direction. The stiffness parameters K_{s_p} and K_{s_n}, damping parameters B_p, and B_n are considered for positive and negative twist angle $\Delta\theta$, respectively. Hence, the piece-wise function for the output torque τ is given as:

$$\tau = f(\Delta\theta) = \begin{cases} J\ddot{\Delta\theta} + B_n\dot{\Delta\theta} + K_{s_n}\Delta\theta & \Delta\theta < 0 \\ J\ddot{\Delta\theta} + B_p\dot{\Delta\theta} + K_{s_p}\Delta\theta & \Delta\theta \geq 0 \end{cases} \tag{1}$$

The inertia J is considered the same for both directions of input torque, τ, since the cross-sectional geometry of the flexible shaft is the same for both directions of torque.

2) Parallel Elastic Effect: For the obstacle or joint the flexible shaft is passing through, it behaves like a helical torsional spring under bending, providing parallel elasticity, in parallel to the preceding joint motor causing the bend as shown in Figure 4 b). Since there are many cascaded helical springs in serial and parallel fashion, it is not easy to develop a model based on it. However, using the bending formula of Euler Beam Theory, it can be generalized concerning material and physical dimensions. Hence, bending stiffness K_b is given by:

$$K_b = \frac{EI}{L} = \frac{M}{\varphi_B} \tag{2}$$

where, E is the Young's modulus, I is the second polar moment of inertia, L is the length of the rod, M is the moment applied for φ_B bending deflection. Empirically, the effective bending stiffness of a flexible shaft is calculated by measuring moment, M and deflection, φ_B. The equation (2) is, though, theoretically valid only for small deflections and linear in a moment-deflection relationship, the empirical approximation for flexible shaft proves to be nearly linear (discussed in section III-B2), making its utility valid.

III. Experimental Investigation

A. Experimental Setup

The experimental setup (Figure 5) employs a Maxon brushless DC motor (Catalog no. 167178) with a planetary gearbox (Gear ratio 91:1, catalog no. 203125) for series elasticity. Flexible shafts from SSWhite UK Ltd. (MasterFLex) with diameters ranging from 4-13 mm and lengths from 235-535 mm are used. Nine flexible shafts with variable diameters and lengths are chosen for benchmarking, covering a stiffness range from low to high, with a bending angle capability of up to $\varphi_B = 90°$. A DBRK-20 analog torque sensor (ETH-Messtechnik) with a 20 Nm measurement range is utilized for torque measurement, fixed at the load end of the flexible shaft. An optical encoder EM2 from US Digital measures the twist angle $\Delta\theta$ between the motor's output and the input of the flexible shaft.

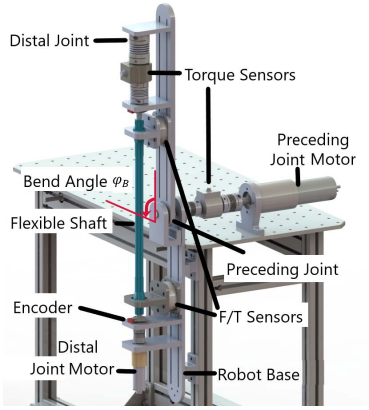

Fig. 5. Experimental Setup

A maxon brushed DC motor (Catalog no. 353295) with a planetary gearbox (Gear ratio 51:1) is connected via a torque sensor to the joint between two links for parallel elasticity (see Figure 5). The setup utilizes Beckhoff IO modules, Maxon Driver EPOS4, and TwinCAT EtherCAT for data acquisition. Bellow shaft couplings compensate for axis misalignment without backlash. Flexible shaft ends are fixed to prevent linear contraction due to helical buckling.

A chirp signal ranging from 0.5 to 20 Hz is inputted to the torque controller for each flexible shaft, with amplitudes based on their nominal torque. The desired torque profiles are followed as the bending angles vary from 0° to 90° in 15° increments. Implementation utilizes MATLAB Simulink and TwinCAT shell in Microsoft Visual Studio.

B. Experimental Results

1) Series Stiffness: Figure 6 shows the output torque, τ of the flexible shaft (Diameter = 9 mm, Length = 450 mm)

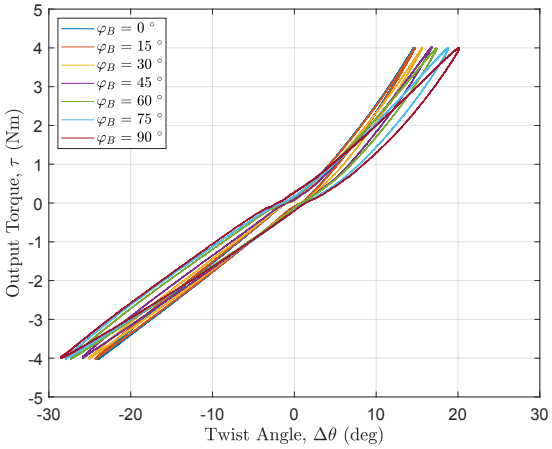

Fig. 6. Series Stiffness Results - D = 9 mm Length = 450 mm

alongside the deflection by twist angle, $\Delta\theta$ for various bending angles, φ_B. The inertial and damping terms from equation (1) are identified to be negligible for series stiffness effect with the change of input frequency from 0.5 to 20 Hz. This can be identified by no change of shape of input-output characteristics plot under the change of input frequency in Figure 6. The stiffness term is estimated using the slope of input-output characteristics of output torque and twist angle, $\Delta\theta$. The slope of the torque concerning the twist angle declines with the increase of bending angle consistently for both the positive and negative sides of the twist angle. Increase in bending deformation results in a compromise in torsional stiffness. Being supported by the conduit, the increase in bending angle assists the flexible to keep helical buckling or torsional instability below the critical stage.

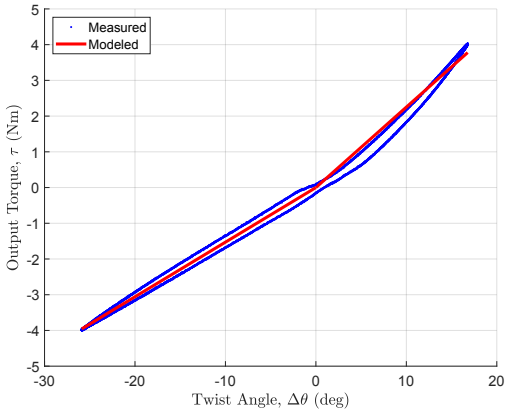

Fig. 7. Model vs. Measured Input-Output Characteristics at $\varphi_B = 45°$.

In Figure 6, one can see the non-identical behavior at both sides of the twist angle due to the winding or unwinding of the outermost layer of the flexible shaft. The unwinding of the outer layer of coils results in a slight decline in the stiffness of the flexible shaft compared to its winding direction as coil jamming lessens effectively by a coil. Hysteresis increases with the increase in bending angle, φ_B, as the deformation of the flexible shaft increases in the form of torsion, bending, and helical buckling. Figure 7 shows the model of equation (1) fitted separately for both the positive and negative twist angle, $\Delta\theta$. The fit of model on the positive side of twist angle, $\Delta\theta$ is less accurate in comparison to the negative side. This owes to the asymmetrical nature of the flexible shaft and relatively different internal friction on each side. On the positive side of the twist angle, there is a dominant internal friction effect due to the outermost coil tightly compressing the internal coils. A single-order polynomial is considered for finding the stiffness characteristics of the flexible shaft on each side due to their quasi-linear behavior. Internal friction analysis due to the stresses between coil layers is left out for brevity. In Figure 7, the experiment and modeled characteristics demonstrate that the flexible shaft mainly behaves as an elastic element and has less dominant inertia and damping terms with respect to those of motor and load as there is no change of shape of the graph under the change of velocity, acceleration and frequency of input signal.

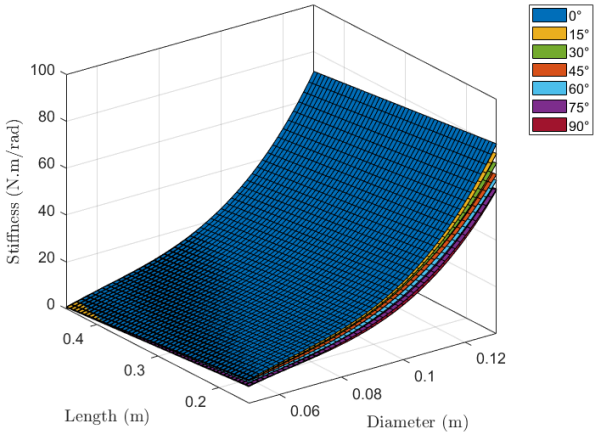

Fig. 8. Empirical Formulation for Series Elastic Effect.

The same set of fits is achieved for the other eight flexible shafts, providing us a map of change of torsional stiffness for diameter, D, length, L, and bending angle, φ_B. Using the experimental stiffness values for both the positive and negative side of twist angle and their rate of change to diameter, length, and bending angle, a set of 3-D surfaces are generated using non-linear regression as shown in Figure 8. A general equation for torsional stiffness, K_s, with coefficient values for both positive and negative twist angle, is given as:

$$K_s(D, L, \varphi_B) = p_0 + p_1 D + p_2 D^2 + p_3 D^3 + p_4 L + p_5 \theta + p_6 D^2 \varphi_B \quad (3)$$

TABLE I
COEFFICIENTS FOR STIFFNESS K_{s_p} AND K_{s_n} AS $f(D, L, \varphi_B)$.

	$\mathbf{Coeff_p}$	$\mathbf{Coeff_n}$	$\varphi_\mathbf{B}$	$\mathbf{RMSE_p}$	$\mathbf{RMSE_n}$
p0	-26.97	-54.959	0 °	0.51	0.98
p1	1.569e03	2648.8	15 °	0.61	1.01
p2	-2.13e04	-3.6e04	30°	0.71	0.89
p3	1.21e05	0.18	45°	0.72	0.78
p4	-27.461	-0.024	60 °	0.62	0.69
p5	0.028	0.064	75°	0.39	0.68
p6	-13.723	1.16	90 °	0.17	0.62

Using the equation (3), one can estimate a torsional stiffness of a flexible for a fixed diameter,D, length,L and bending

angle,φ_B for an optimal design of series stiffness for the desired robotic application. Here, p_i are the coefficient provided in Table I for the positive and negative side of the twist angle, $\Delta\theta$. In equation (3) and Figure 8, a non-linear relationship of diameter, D and linear relation of length, L to stiffness, K_s can be observed, declining linearly with the bending angle,φ_B. This information is not available in the manufacturer's catalog [17], thus fulfilling the required design information.

2) Parallel Stiffness: Figure 9 shows the measurement of the moment, M, with respect to a deflection or bending angle φ_B at the joint. This result is achieved by continuously bending the flexible shaft with and without torsion in both directions of flexible shaft bending. Torsion-ed bending results in no considerable difference from the non-torsion-ed bending. Due to the straight/vertical initial configuration of the flexible shaft, the bending stiffness of the flexible shaft assists the joint motor in lifting its gravitational load with the increase in its bending angle. The results show non-linearity with an increase in the bending angle due to the bend angle approaching the critical bending of the flexible shaft, where bending more takes a considerable torque to achieve a small amount of bend.

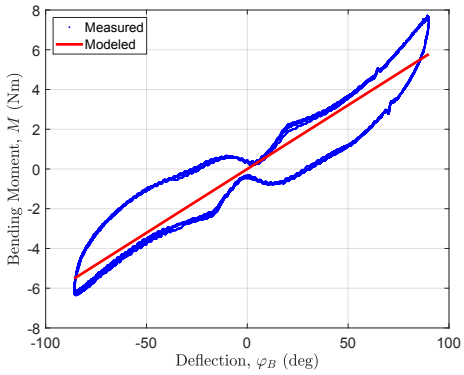

Fig. 9. Parallel Stiffness Result - D = 9 mm Length = 450 mm.

Figure 9 also shows an evident hysteresis region from a no-bend to bend configuration and on return. This is the behavior of flexible conduit made of rubber and elastic coil used outside the flexible shaft. The visco-elastic rubber generates a considerable region of hysteresis, causing the parallel stiffness effect, a problem in joint control for torque mode. This requires hysteresis estimation to overcome the problem, which is left out for brevity in this paper.

Though approaching non-linearity at extreme bending angles, a linear fit for approximation is achievable between moment, M, and deflection, φ_B as shown in Figure 9. For simplicity, linear regression is used to understand the relationship between bending stiffness of the flexible shaft with the change in length and diameter. This simplifies how the parallel spring torque is affected on the preceding joint with the flexible shaft's change of diameter and length.Hysteresis modeling is required to reduce the residual errors for the viscous nature of this parallel stiffness effect. A map of parallel stiffness is achieved for the same set of experiments for variable diameters and lengths for eight flexible shafts. Figure 10 shows a 3-D surface generated using non-linear regression for the set of bending stiffness values and its trend for changes in diameter

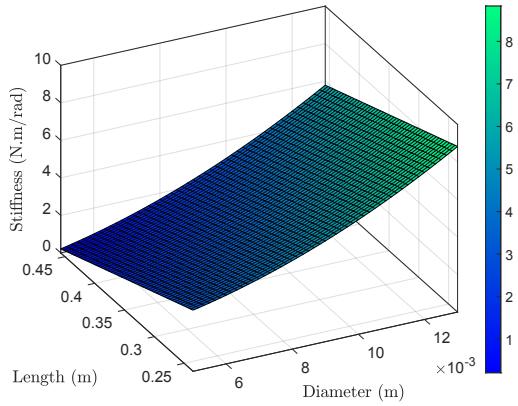

Fig. 10. Empirical Formulation of Parallel Elastic Effect.

and length. A general equation for bending/parallel stiffness is given as:

$$K_b(D, L) = p_0 + p_1 D + p_2 L + p_3 D^2 + p_4 DL \qquad (4)$$

Using the equation (4) and coefficient values,p_i in Table II, an optimal parallel stiffness is achievable by selecting the diameter,D, and length,L, of flexible shaft as per the design requirements of the robot. The non-linear and linear relation of the diameter, D and length, L is observed in the experimental results and surface plot with respect to bending stiffness values.

TABLE II
COEFFICIENTS FOR BENDING/PARALLEL STIFFNESS K_b AS $f(D, L)$.

Coefficient	**p0**	**p1**	**p2**	**p3**	**p4**	**RMSE**
Values	5.734	-60.3	-13.72	-0.014	4203	0.59

IV. ROBOT BASED ON FLEXIBLE SHAFT

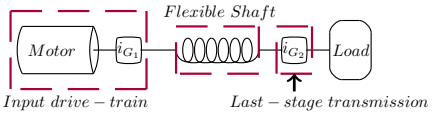

Fig. 11. Flexible Shaft Based Remote and Elastic Actuator.

Considering the dimensions and joint requirements of KUKA LBR IIWA, a three DOF robot with similar kinematics is designed using a flexible shaft as a remote actuator for a third joint, with a rated torque of 66 Nm and speed of 1.31 rad/s. An actuator design based on flexible shaft transmission can constitute different possibilities, as shown in Figure 11. $i_{G_1} = 1, i_{G_2} \neq 1$ allows for a selection of thin, flexible shaft with a gearbox to be placed at joint 3, causing not a considerable advantage against direct actuation. $i_{G_1} \neq 1, i_{G_2} = 1$ could be ideal for low moving mass but requires a very thick flexible shaft for high joint torque requirements, making the bending compliance high in magnitude and non-linear due to high minimum bending radius values. $i_{G_1} \neq 1, i_{G_2} \neq 1$ is a favorable choice to achieve remote actuation with a low

TABLE III
DESIGN SPECIFICATIONS OF ROBOT BASED ON FLEXIBLE SHAFT.

Payload (kg)	**Reach** (mm)	$\mathbf{L_1}$ (mm)	$\mathbf{L_2}$ (mm)	$\mathbf{L_3}$ (mm)
15	820	200	420	400
$\dot{\mathbf{q}}_{\mathbf{1}}$ & $\dot{\mathbf{q}}_{\mathbf{2nom}}$ (deg/s)	$\dot{\mathbf{q}}_{\mathbf{3nom}}$ (deg/s)	$\tau_{\mathbf{1nom}}$ (Nm)	$\tau_{\mathbf{2nom}}$ (Nm)	$\tau_{\mathbf{3nom}}$ (Nm)
85	75	31	138	67

moving mass of a robot as it allows for mass distribution among two gearboxes.

The third joint actuation design is attained so that a single-stage gearbox, i_{G2} is used on joint 3 , to attain low mass and high back-drivability. The rest of the transmission ratio is achieved through i_{G1} placed in the robot's base. The actuator motor with gearbox can be placed on joint 2 and link 2. However, the parallel stiffness effect is not attained at preceding joint 2, and the moving mass is not reduced as effectively as placing it on link 1.

A. Mechanical Design

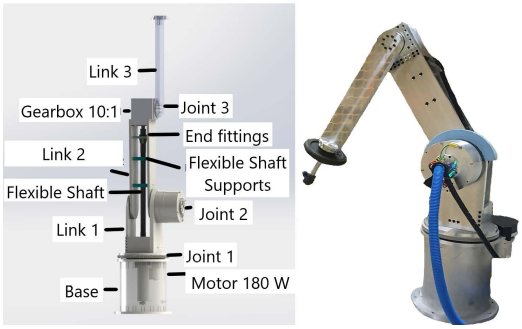

Fig. 12. Robot Based on Flexible Shaft.

1) Selection of Flexible Shaft: As a remote actuator for a robotic application, a flexible shaft can be selected based on required torque-speed requirements. However, as a series or parallel elastic actuation, one can optimize a flexible shaft selection for either series or parallel elasticity, not both at once. As a remote actuator, the online technical characteristics provided by SSWhite Technologies [17] serve as a good reference. However, this source provided non-consistent results for the elastic characteristics of the shaft as per our experimental results. An essential nature is worthy of notice in [17] that the nominal ratings of the flexible shaft are a function of its diameter only, which is non-identical with a rigid shaft. Hence, one can select the diameter, D_{des} of a flexible shaft based on the nominal rating required and vary the length, L_{des} of the shaft in the robot's dimensional limit range, $[L_{min}, L_{max}]$ to achieve the desired stiffness.

Using algorithm 1, one can estimate the desired series or parallel elasticity,K_{des} for a flexible shaft using equation (3) or (4). In the case of parallel elasticity, it indirectly depends on the series elasticity through the diameter and length selected. For series stiffness, once a straight configuration's desired stiffness is achieved, the bending angle parameter,φ_B can be changed to determine the stiffness change by bending using

Algorithm 1 Estimation of Series/Parallel Elasticity.

$D_{des} \leftarrow D(\tau_{req}, \omega_{req})$
$L \leftarrow [L_{min}, L_{max}]$
$L_{des} \leftarrow rand(L)$
$N_{itr} \leftarrow size(L)$
$\delta \leftarrow K_{des} - K$
while $i = 1 \leq N_{itr}$ **do**
  if $\delta > 0$ **then**
    $L_{des} = L_{des} + \frac{L_{max} - L_{min}}{N_{itr}}$
  else
    $L_{des} = L_{des} - \frac{L_{max} - L_{min}}{N_{itr}}$
  end if
  $i++$
end while

equation (3). Due to the non-linear relationship of diameter and implicit equations, (3) and (4), an iterative approach is taken in Algorithm I.

Due to empirical fitting, there lies an error in both models as curve fitting is achieved to minimize the root means square error (RMSE). Due to the limited number of flexible shafts tested, it is a compromise to make for the estimation of flexible shafts' stiffness parameters. A masterflex with a diameter of 9 mm and a flexible shaft's length of 450 mm (end-to-end length of 550 mm) is selected for the prototyping.

2) Robot Design: For 3 DOF robot design, the base joint 1 has a slew ring run by a set of gears actuated by a Tinsmith erob80 actuator with a harmonic reducer of 50:1. Joint 2 is actuated using a tinsmith actuator erob142 with harmonic reducer of 100:1. Joint 3 is actuated using a brushless maxon motor with gear ratio 16:1 place at link 1 rotating inside the base of the robot with the rotation of joint 1. At the output of the joint 3 actuator, a flexible shaft is connected with an encoder installed in between. The flexible shaft routes through joint 2 and connects to a hypoid gearbox from NIDEC with a reduction of 10:1. Supports along the length support the flexible shaft to keep its deformation in a plane of bending only. Table III shows the design specifications of the robot. Figure 12 shows the CAD and the real robot with a payload.

Hypoid gearbox is selected over the right-angle transmission of the worm, bevel, and bevel plus planetary gearbox due to its high efficiency and compact nature. The robot is designed to test the remote actuation using a flexible shaft as an initial working prototype.

B. Dynamic Model

De Luca et al. [18] discusses the dynamic model for the flexible/elastic joint-based robotic manipulators in detail. The general form of the model is given by:

$$M_{SEA}(q)\ddot{q} + S(q)^T\ddot{\theta} + C(q,\dot{q})\dot{q} + C_1(q,\dot{q},\ddot{\theta})\dot{q} + g(q) + K(q-\theta) = 0$$

$$S(q)\ddot{q} + B(\theta)\ddot{\theta} + C_2(q,\dot{q})\dot{q} + K(\theta - q) = \tau$$

Here, q is the generalized symbol for joint coordinates; θ is the actuator output coordinates. τ is the motor torques

for the joints. $B(\theta)$ is the constant inertia matrix with rotors inertial components. $M_{SEA}(q) = M_L(q) + M_R(q) + S(q)B(\theta)^{-1}S(q)^T$ is the inertia matrix for flexible joints-based manipulator with rigid links, M_L is the link inertia matrix and M_R is the motor's rotor masses and inertial components along other local axes. $S(q)$ is the coupling matrix between rotors and links rigid bodies. $C_1(q,\dot{q},\dot{\theta})$ and $C_2(q,\dot{q})$ are centrifugal and Coriolis terms due to the coupling between rotors and links rigid bodies caused by the elastic element. $K.(q-\theta) = \tau_{spring}$ is the spring torque with stiffness, K and deflection, $\theta - q$. Using the above two equations, it can be reduced to:

$$M_{SEA}(q)\ddot{q} + S(q)^T\ddot{\theta} + S(q)\ddot{q} + B(\theta)\ddot{\theta} + C(q,\dot{q})\dot{q} + C_1(q,\dot{q})\dot{q} + C_2(q,\dot{q})\dot{q} + g(q) = \tau \quad (5)$$

For a robot with both series and parallel elasticity at every joint, the dynamic model of the robot is given by:

$$M_{SEA}(q)\ddot{q} + S(q)^T\ddot{\theta} + S(q)\ddot{q} + B(\theta)\ddot{\theta} + C(q,\dot{q})\dot{q} + C_1(q,\dot{q})\dot{q} + C_2(q,\dot{q})\dot{q} + g(q) + K_{PEA}q = \tau \quad (6)$$

Where K_{PEA} is the parallel stiffness matrix for a parallel stiffness at every robot joint. For joint motors at joints 1 and 2, the coupling between the rotor of joint 2's motor and the link 1 is neglected due to orthogonal axes. For the case of remote actuation, where the rotor's rotation axis is orthogonal to the joint 2's axis, the coupling between the rotor and link is also nullified. In the case of the robot based on the flexible shaft, the axis of rotation of the motor for joint 3 is perpendicular to the second joint's axis. However, link 1's axis is aligned with joint 3's motor, which introduces a coupling between them. Also, the mass of the actuator for joint 3 being placed at the center of link 1 introduces additional inertia given as $m_{r_3}r_3^2$. The joint stiffnesses of harmonic drives at Joints 1 and 2 are considered to be nearly rigid and their deflections goes to zero, $q - \theta \to 0$. However, one can introduce a stiffness value for harmonic drives in the model easily. Thus, the matrices are given as (in Coordinate Form Notation):

$$K_{SEA_{3X3}} = \{(1,1,\infty),(2,2,\infty),(3,3,K_s i_{G_2}^2)\}$$
$$M_{R_{3X3}} = \{(1,1,m_{r_3}r_3^2)\} \quad ; \quad S_{3X3} = \{(1,3,I_{r3-zz}i_{G_1})\}$$
$$B_{3X3} = \{(1,1,I_{r1,zz}i_1^2),(2,2,I_{r2,zz}i_2^2),(3,3,I_{r3,zz}i_{G_1}^2)\}$$

Here, K_s is the series stiffness of the flexible shaft, and i_{G_2} is the gear ratio of the hypoid gearbox. $m_{r_3}r_3^2$ is the inertial component of the rotor for joint 3 along the joint 1's axis. Masses of other rotors are considered to be included with the links. $I_{ri,zz}$ is the inertia of the rotor of joints 1,2 and 3 along the local z-axis; i_1 and i_2 are the transmission ratios of motors for joints 1 and 2. Since S is a constant matrix, C_1 and C_2 are zero. Due to the presence of parallel stiffness only along the second joint of the robot, K_{PEA} matrix is given as: $K_{PEA_{3X3}} = \{(2,2,K_b)\}$. Hence, for the case of robot based on flexible shaft, the equation (6) is given as:

$$M_{SEA}(q)\ddot{q} + S(q)^T\ddot{\theta} + S(q)\ddot{q} + B(\theta)\ddot{\theta} + C(q,\dot{q})\dot{q} + g(q) + K_{PEA}q = \tau \quad (7)$$

C. Control of Flexible Shaft

Cianca et al. [13] proposed a control methodology for a flexible shaft based actuator using an empirical formulation of the Fourier series, incorporating the radius of curvature, R. The same approach is adapted for the bending angle, φ_B, instead of the radius of curvature, R due to ease of measurement. Our experimental analysis has shown that inertia and damping coefficients are quite small compared to the dominant inertia and damping coefficients of load and motor due to no-change of shape of input-output characteristics in Figure 6 with the change of input frequency.

Using equation (1), the set of coefficients K_{s_n} and K_{s_p} are identified for each direction of twist angle using the experimental data shown in Figure 6. These coefficients' trend of decline due to bending angle is mapped using a polynomial fit to include the effect of bending angle,$\varphi_B = [\frac{-2\pi}{3}, \frac{2\pi}{3}]$. Due to the small magnitude of J and B terms, the equation (1) can be simplified and the adapted equation for various bending angles is given as:

$$\tau = f(\Delta\theta, \varphi_B) = \begin{cases} K_{s_n}\Delta\theta f_{pn}(\varphi_B) & \Delta\theta < 0 \\ K_{s_p}\Delta\theta f_{pp}(\varphi_B) & \Delta\theta \geq 0 \end{cases} \quad (8)$$

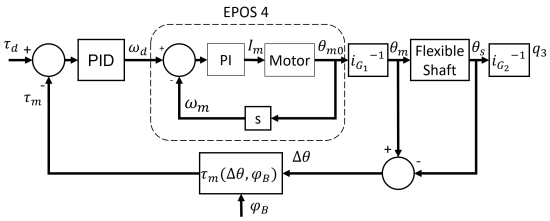

Fig. 13. Low Level Control of flexible shaft based actuator.

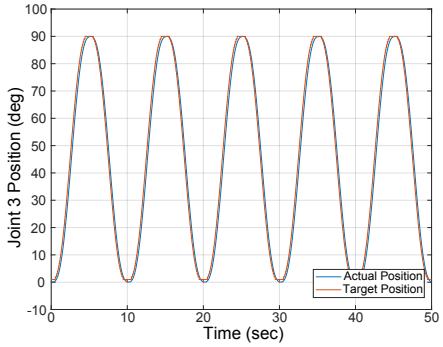

Fig. 14. Actual vs. Desired Position Tracking of Joint 3.

Figure 7 shows the linear model fit based on equation (8) on a bending angle $\varphi_B = 45°$. The low-level control of flexible shaft-based actuator is implemented using the equation (8), as shown in Figure 13. The twist angle $\Delta\theta$ is measured using a set of two encoders before and after the flexible shaft, which provided the values of θ_m and θ_s. A desired torque for a reference trajectory of joint position is fed to the low-level control block of a flexible shaft-based actuator to attain the desired position tracking. The bending angle values φ_B are measured through the joint encoder of joint 2 and fed into the

low-level controller. At a motor driver level, a speed controller is implemented using the EPOS4 motor driver. A simple PID controller translates the difference in desired τ_d and actual modeled torque τ_m values at joint 3 to the desired angular speed for the motor ω_d.

Joint 3 utilizes the joint encoder as a feedback sensor for position control with the proposed controller. Figure 14 illustrates the tracking of the flexible shaft-based actuator's actual position to the desired sinusoidal position within a 0 to 90° joint angle range. Well-tuned parameters enable good trajectory tracking by the controller. However, inaccuracies in the model arise from hysteresis in the torque-twist angle profile of the flexible shaft. Additionally, non-linearity in hypoid and planetary gearboxes, along with non-collocated feedback sensors, can lead to instability at high disturbances, requiring adjustment of tuning parameters for different loads.

V. Discussion and Conclusion

The paper discusses the characteristics and usefulness of flexible shafts in robot arms. Experiments varied shaft length and diameter to understand their characteristics. Torsional stiffness decreases linearly with bending angle and length but shows a nonlinear relationship with diameter. 3-D surface maps of torsional stiffness changes were approximated using nonlinear regression. Empirical formulations estimate torsional and bending stiffness based on diameter, length, and bending angle. Hysteresis in bending stiffness complicates torque control of preceding robot joints. Like rigid shafts and torsional springs, material characteristics can be accounted for by adjusting polynomial coefficients in stiffness equations (3) and (4).

Using a flexible shaft as an actuator offers several advantages in robot arm design. Its series elastic effect on Joint 3 helps to decouple inertia from its actuation unit on Link 1 and acts as an energy buffer under load [5]. The parallel elastic effect reduces static torque on Joint 2 by approximately 8 Nm, acting as an imperfect gravity compensation [5]. Its remote nature allows mass relocation towards the base while transmitting torque across joints, reducing inertia and energy consumption [9]. Compared to belt/cable pulley systems, it simplifies kinematics without needing additional tensioning mechanisms.

The design, modeling, and control of a robot utilizing flexible shafts were discussed, focusing on optimizing its performance. Future work will concentrate on refining the robot arm's design to maximize the benefits of flexible shafts in remote actuation and elasticity. Special attention will be given to developing hysteresis compensation techniques for accurate torque control in robot joints, particularly for series and parallel elasticity. Understanding the relationship between internal stresses in flexible shafts and bending angles requires improved physics-based models. For series stiffness, rate-independent hysteresis can be effectively modeled using the Maxwell Fit Model [19], while for parallel stiffness, addressing the viscous nature of the conduit material is essential, possibly through improved modeling using rate-dependent hysteresis modeling [20].

References

[1] D. Vischer and O. Khatib, "Design and development of high-performance torque-controlled joints," *IEEE Transactions on Robotics and Automation*, vol. 11, no. 4, pp. 537–544, 1995.

[2] G. Hirzinger, A. Albu-Schaffer, M. Hahnle, I. Schaefer, and N. Sporer, "On a new generation of torque controlled light-weight robots," in *Proceedings 2001 ICRA. IEEE International Conference on Robotics and Automation*, vol. 4, 2001, pp. 3356–3363 vol.4.

[3] A. O. Albu-Schäffer, S. Haddadin, C. Ott, A. Stemmer, T. Wimböck, and G. Hirzinger, "The dlr lightweight robot: design and control concepts for robots in human environments," *Ind. Robot*, vol. 34, pp. 376–385, 2007.

[4] G. Pratt and M. Williamson, "Series elastic actuators," in *Proceedings 1995 IEEE/RSJ International Conference on Intelligent Robots and Systems. Human Robot Interaction and Cooperative Robots*, vol. 1, 1995, pp. 399–406 vol.1.

[5] T. Verstraten, P. Beckerle, R. Furnémont, G. Mathijssen, B. Vanderborght, and D. Lefeber, "Series and parallel elastic actuation: Impact of natural dynamics on power and energy consumption," *Mechanism and Machine Theory*, vol. 102, pp. 232–246, 2016.

[6] D. W. Robinson, "Design and analysis of series elasticity in closed-loop actuator force control," Ph.D. dissertation, Massachusetts Institute of Technology, 2000.

[7] S. Wolf, O. Eiberger, and G. Hirzinger, "The dlr fsj: Energy based design of a variable stiffness joint," in *2011 IEEE International Conference on Robotics and Automation*, 2011, pp. 5082–5089.

[8] W. T. Townsend and J. K. Salisbury, "Mechanical design for whole-arm manipulation," in *Robots and Biological Systems: Towards a New Bionics?*, P. Dario, G. Sandini, and P. Aebischer, Eds. Berlin, Heidelberg: Springer Berlin Heidelberg, 1993, pp. 153–164.

[9] Y.-J. Kim, "Anthropomorphic low-inertia high-stiffness manipulator for high-speed safe interaction," *IEEE Transactions on Robotics*, vol. 33, no. 6, pp. 1358–1374, 2017.

[10] T. Lens and O. von Stryk, "Investigation of safety in human-robot-interaction for a series elastic, tendon-driven robot arm," in *2012 IEEE/RSJ International Conference on Intelligent Robots and Systems*, 2012, pp. 4309–4314.

[11] M. Zinn, O. Khatib, and B. Roth, "A new actuation approach for human friendly robot design," in *IEEE International Conference on Robotics and Automation, 2004. Proceedings. ICRA '04. 2004*, vol. 1, 2004, pp. 249–254 Vol.1.

[12] D. Shin, I. Sardellitti, and O. Khatib, "A hybrid actuation approach for human-friendly robot design," in *2008 IEEE International Conference on Robotics and Automation*, 2008, pp. 1747–1752.

[13] D. Rodriguez-Cianca, C. Rodriguez-Guerrero, T. Verstraten, R. Jimenez-Fabian, B. Vanderborght, and D. Lefeber, "A flexible shaft-driven remote and torsionally compliant actuator (rtca) for wearable robots," *Mechatronics*, vol. 59, pp. 178–188, 2019.

[14] D. Kim, D. Lee, S. Joe, B.-I. Lee, and K.-J. Cho, "The flexible caterpillar based robotic colonoscope actuated by an external motor through a flexible shaft," *Journal of Mechanical Science and Technology*, vol. 28, no. 28, 2014.

[15] Y. Kobayashi, Y. Sekiguchi, T. Noguchi, Y. Takahashi, Q. Liu, S. Oguri, K. Toyoda, M. Uemura, S. Ieiri, M. Tomikawa, T. Ohdaira, M. Hashizume, and M. G. Fujie, "Development of a robotic system with six-degrees-of-freedom robotic tool manipulators for single-port surgery," *The International Journal of Medical Robotics and Computer Assisted Surgery*, vol. 11, no. 2, pp. 235–246, 2015. [Online]. Available: https://onlinelibrary.wiley.com/doi/abs/10.1002/rcs.1600

[16] Q. Liu, X. Gu, N. Tan, and H. Ren, "Soft robotic gripper driven by flexible shafts for simultaneous grasping and in-hand cap manipulation," *IEEE Transactions on Automation Science and Engineering*, vol. 18, no. 3, pp. 1134–1143, 2021.

[17] S. W. Technologies, "Technical characteristics of commercial flexible shafts," *https://www.sswhite.net/copy-of-bi-directional-english*, 2020.

[18] A. De Luca and W. J. Book, *Robots with Flexible Elements*. Cham: Springer International Publishing, 2016, pp. 243–282. [Online]. Available: https://doi.org/10.1007/978-3-319-32552-1_11

[19] H. Zhang, S. Ahmad, and G. Liu, "Modeling of torsional compliance and hysteresis behaviors in harmonic drives," *IEEE/ASME Transactions on Mechatronics*, vol. 20, no. 1, pp. 178–185, 2015.

[20] M. Al Janaideh and P. Krejčí, "Inverse rate-dependent prandtl–ishlinskii model for feedforward compensation of hysteresis in a piezomicropositioning actuator," *IEEE/ASME Transactions on Mechatronics*, vol. 18, no. 5, pp. 1498–1507, 2013.